High-Resolution Observations with MU Radar of a KH Instability Triggered by an Inertia–Gravity Wave in the Upper Part of a Jet Stream

H. LUCE

Laboratoire de Sondages Electromagnétiques de l'Environnement Terrestre, Université de Toulon et du Var, CNRS, La Garde, France

G. HASSENPFLUG, M. YAMAMOTO, AND S. FUKAO

Research Institute for Sustainable Humanosphere, Kyoto University, Uji, Japan

K. SATO

Department of Earth and Planetary Science, University of Tokyo, Tokyo, Japan

(Manuscript received 13 November 2006, in final form 28 September 2007)

ABSTRACT

Kelvin–Helmholtz (KH) instability is likely one of the most important sources of clear-air turbulence in the lower atmosphere. It produces billows, which mix and transport heat and materials vertically in the stably stratified atmosphere. Billows can also dissipate energy; therefore they can affect the larger-scale dynamics. While only a few direct observations have been reported in the tropopause region, in this work the authors report very detailed observations of billow structures around 16-km altitude, in the upper part of the jet stream. Observations were made with very high frequency (VHF)-band mid- and upper-atmosphere (MU) radar (Shigaraki, Japan; 34.85°N, 136.10°E) whose height resolution was improved with a range-imaging technique. KH billow structures were observed for at least 2 h and were found to have horizontal wavelengths of about 5.3 km and vertical extents between 0.5 and 1.0 km. Analysis of wind and temperature profiles measured by radiosondes launched from nearby meteorological stations indicated the presence of nearly monochromatic disturbances, likely due to a dominant inertia–gravity wave (IGW) superimposed on the background wind field. The presence of the IGW was also confirmed by analysis of wind profiles measured by the MU radar just before the KH billows were detected by the observations in range-imaging mode. The IGW, with vertical and horizontal wavelengths of about 3.5 and 600 km, respectively, may have been a direct radiation from the jet stream, as suggested by recent works, and likely played a major role in the onset of the observed KH instability.

1. Introduction

Kelvin–Helmholtz (KH) instability is likely one of the dominant mechanisms generating small-scale clear-air turbulence in the stable atmosphere (e.g., Browning and Watkins 1970; Hines 1972). Turbulence can be responsible for vertical transport of heat and materials between the troposphere and the stratosphere through intense mixing, particularly in the sheared regions of meteorological upper-level fronts and tropopause folds at midlatitudes (e.g., Shapiro 1980; Bertin et al. 2001; Koch et al. 2005; Gavrilov et al. 2006). KH instability may also cause aircraft hazards (Ralph et al. 1997; Clark et al. 2000).

KH billows result from dynamic instability produced by sufficiently strong wind shear in a statically stable flow. In the real atmosphere, KH billows have often been observed using, for example, high range–resolution frequency modulated continuous wave (FMCW) radars and acoustic sounders near the sheared inversion of the planetary boundary layers at

Corresponding author address: H. Luce, Laboratoire de Sondages Electromagnétiques de l'Environnement Terrestre, Université de Toulon et du Var, CNRS, La Garde 83957, France.
E-mail: luce@lseet.univ-tln.fr

DOI: 10.1175/2007JAS2346.1

the top of stratiform clouds, and less often, in the upper-tropospheric jet streams near the tropopause at 10–11 km (see the review by Gossard 1990). Owing to their high sensitivity, very high frequency (VHF; 30–300 MHz) stratosphere–troposphere (ST) pulsed Doppler radars can provide observations within the tropopause region, up to 20–25 km. Contrary to UHF (300–3000 MHz) radars, VHF ST radars are not only sensitive to turbulent irregularities but also to laminar and thin stable humidity and temperature gradient sheets. The latter should be responsible for aspect-sensitivity at VHF (i.e., for enhanced echo power along the vertical line of sight with respect to oblique looking directions). On the other hand, turbulent structures are believed to produce nearly isotropic scattering at VHF, at least when turbulent mixing is intense. With their typical range resolutions of 150 m, and a time resolution of a few minutes, VHF ST radars are thus a unique tool for studying a variety of phenomena including winds, meteorological fronts and instabilities, and inertia–gravity waves (IGWs). However, such standard resolutions are still not sufficient for direct observations of KH billows or waves, which usually range in spatial scale from a few meters to several hundred meters, with very short periods (on the order of a few minutes or less). Hence, KH billow detection can only be inferred from measurements of line-of-sight velocities made with time resolution on the order of 10 s (e.g., Klostermeyer and Rüster 1980; Chilson et al. 1997). At UHF, only powerful radars such as the French PROUST radar could glimpse such structures in reflectivity maps of the lower stratosphere (F. Bertin 2006, personal communication).

In addition to the need for a high time resolution, the range resolution of VHF ST radars also needs to be improved for resolving the KH billow structures and their development in time. In this work, this was achieved with a newly developed range-imaging technique based on frequency diversity (Palmer et al. 1999; Luce et al. 2001). The 46.5-MHz middle and upper atmosphere (MU) radar, located in Japan (34.85°N, 136.10°E), was upgraded in March 2004 for operating in this high–vertical resolution mode: (i) five frequencies spanning a bandwidth of 1 MHz could be switched pulse to pulse and (ii) the signals collected at these frequencies were processed to estimate the range brightness (related to power) distribution using the nonparametric adaptive Capon filter-bank method (Capon 1969). [This method has been proven to be efficient for improving the range resolution when signal-to-noise ratio (SNR) significantly exceeds 0 dB (Palmer et al. 1999; Luce et al. 2001).]

In section 2, we briefly describe the experimental setup and our observations of KH billows. In section 3, we discuss a possible source of KH instability, and conclusions are given in section 4.

2. KH instability observations with the MU radar

MU radar observations using the range-imaging technique were made on 13–16 November 2005, from 2152 LT. The acquisition time for one profile was 33.4 s and one profile was obtained every 16.7 s. The range resolution before Capon processing was 150 m and the observed height ranges extended from 1.05 to 20.10 km above ground level. Observations were made along the vertical line of sight and at 10° off-zenith only, in order to limit the radar's loss of sensitivity. Since horizontal winds cannot be estimated from this configuration, sequences of about 32 min in range-imaging mode were interrupted by observations using a classical 5-beam Doppler beam-swinging (DBS) mode, which took about 4 min to complete with the same range resolution and sampling.

Figure 1 (top) displays height–time intensity power plots (in dB scale) after Capon processing, measured in the vertical beam from 2152 LT 13 November 2005 (marking the start of the range-imaging experiment) to 2358 LT, and from 11.7- to 18.6-km altitude. Gaps in the images correspond either to the observation periods in DBS mode or to interruptions in radar operation. The white spot around 16 km at minute 2 likely results from an airplane echo and should be discarded. Bright horizontal lines can also be noted, especially in the absence of echoes. These result from a systematic correction of the radar range-weighting function, which produces such an artifact at the edges of the range gates when the noise power dominates (e.g., Luce et al. 2006). Figure 1 (bottom) shows the corresponding plots of vertical velocity, calculated at the initial range resolution of 150 m by incoherently averaging the Doppler spectra obtained at the five frequencies. Missing values correspond to insufficient SNR.

The presence of a train of coherent tilted S-shaped structures having periods of a few minutes around the altitude of 15.5 km is evident in Fig. 1. Such structures are poorly depicted when using the standard resolution and do not appear at a standard time resolution of 2.0 min (not shown). The coherent pattern is clearly delimited, especially before minute 10 and after minute 17, where the crest-to-trough amplitude reaches about 1.0 km around 15.5 km. Observations in a range-imaging mode are unfortunately not available before 2152 LT. It is therefore not possible to know when the phenom-

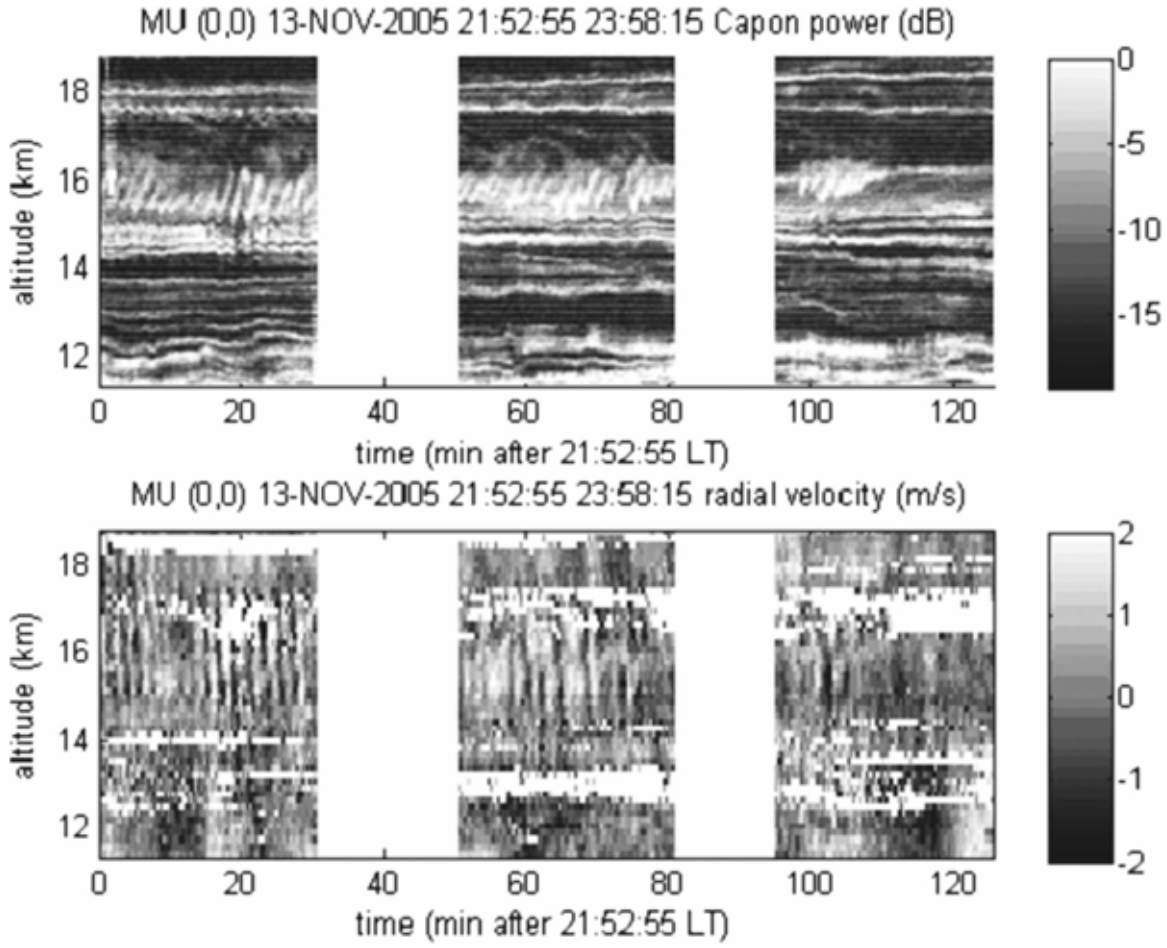

FIG. 1. (top) Height–time power plot after performing Capon processing (dB) between 11.4 and 18.9 km from 2152 to 2358 LT 13 Nov 2005 with the vertically oriented beam. (bottom) The corresponding plots of radial velocity measured with the vertical beam at a range resolution of 150 m.

enon was triggered. The pattern appears intermittently (e.g., the striations suddenly appear and disappear in the third sequence) and the amplitude varies in time. The slope of the axis of the most intense echoes varies accordingly (the larger the amplitude, the steeper the slope).

The height–time intensity plots of vertical wind velocity in Fig. 1 (bottom) reveal large and rapid oscillations around the altitude of the coherent structures. Such velocity fluctuations have often been observed and were interpreted in terms of KH instabilities (e.g., Klostermeyer and Rüster 1980; Chilson et al. 1997). Figure 2 (top left) shows time series of vertical velocity measured at 15.35 and 15.95 km. Their crest-to-trough amplitude exceeds 4 m s^{-1} at 15.97 km. The fluctuations at the two altitudes are approximately in quadrature and the phase shift of about 90° occurs near 15.5 km, as estimated from visual inspection of Fig. 1 (bottom). Thus the coherent structures seen in the power maps are likely related to KH billows. Indeed, the 90° phase shift reveals a critical level of KH instability (e.g., Klostermeyer and Rüster 1980). A spectral analysis of the time series of vertical wind velocity is shown in Fig. 2 (bottom left). The ground-based period T of the main oscillations is about 2.0 min at both altitudes. The mean horizontal wind velocity υ at the height of the KH billows is 44 m s^{-1}, according to the observations in DBS mode performed at 2148 LT (see section 4). The horizontal wavelength is thus $\lambda = \upsilon T \approx 5.3$ km. Since the thickness of the billows ranges from about 0.5 to 1.0 km, an aspect ratio between 5.3 and 10.6 is found. The averaged value is close to the aspect ratio (7.5) expected from the theory for the most unstable wave (e.g., Turner 1973).

Thin and persistent layers are observed above and below the KH billows in Fig. 1. The thickness of these layers can be as small as a few tens of meters (i.e., much thinner than the initial range resolution; Luce et al.

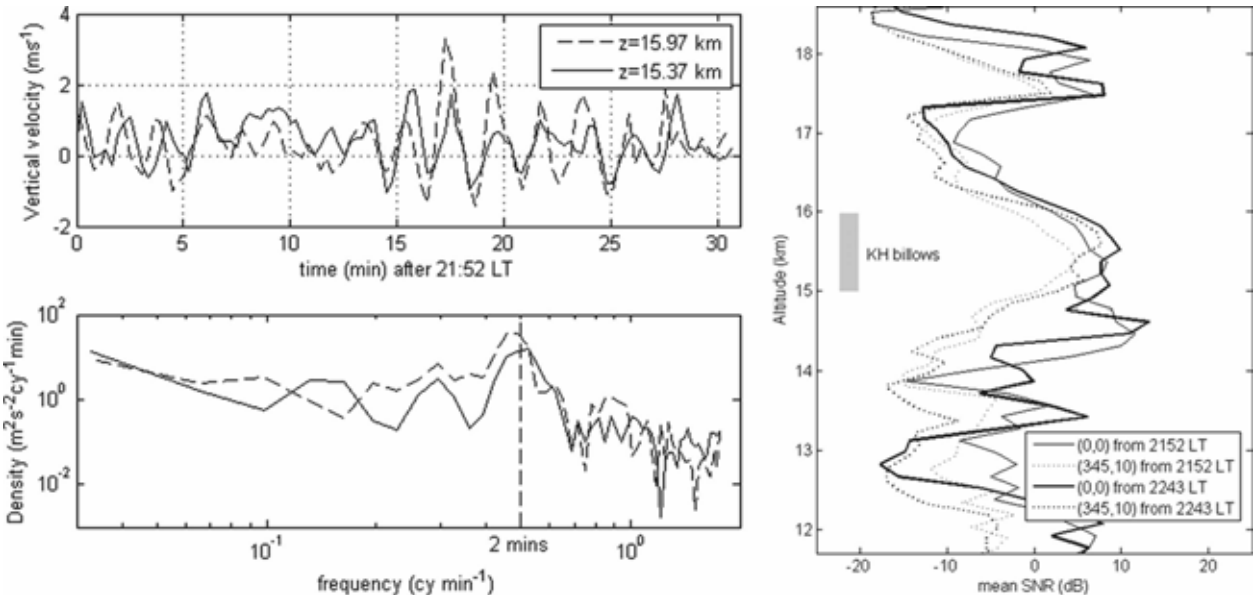

FIG. 2. (top left) Time series of radial velocities measured with the vertical beam at 15.37 km (solid line) and 15.97 km (dashed line). (bottom left) Corresponding velocity spectra. (right) Mean profiles of SNR corresponding to the two first periods and altitude ranges shown in Fig. 1.

2006). Figure 2 (right) shows mean vertical profiles of SNR for both vertical and oblique directions. Time averaging has been performed over two periods from 21:52 to 22:23 LT and from 22:43 to 23:14 LT, corresponding to the first two panels shown in Fig. 1. The thick peaks between 15 and 16 km correspond to the KH billows and have a similar intensity in both directions, suggesting that these structures produce nearly isotropic scattering at the Bragg scale. By contrast, the thin layers below the KH billows (around 14.5 km) are much more aspect-sensitive, indicating a horizontal coherence of the structures (at the half-radar wavelength) so that the quasi-specular reflection mechanism should dominate. It is believed that these thin echoing layers are caused by stable gradient sheets, which can be as thin as a few meters (or less). These may thus correspond to the height ranges where the thin sheets are embedded. In Fig. 1, it is clear that the thin layers oscillate in conjunction with the KH billows, especially when the depth of the billows is maximum (e.g., around minute 20). The period of these oscillations is the same as the period of oscillations of the train of KH billows (2 min), suggesting a direct influence of the KH instability on its nearby stable environment. The oscillations are also associated with fluctuations of power due to the tilts of the stable layers. Interestingly, other wavelike disturbances can be observed on the thin layers below 18 km and the period of the oscillations estimated from a spectral analysis similar to Fig. 2 is 1 min 40 s.

3. A possible source of the KH instability

At the time of observations, the meteorological charts supplied by the Japan Meteorological Agency depicted a strong high-level westerly jet stream flowing with a maximum of about 75 m s^{-1} at an altitude of 12 km (200 mb) over the western Pacific during the period of observations (Fig. 3, top). From cross-sectional latitudinal charts of temperature, the tropopause height above the MU radar was estimated at between 14 and 16 km (150–100 mb). The KH billows were thus produced in the tropopause region. The vertical profiles of meridional and zonal wind components measured by the MU radar in DBS mode at 2148 local time (LT) are shown in Fig. 3 (bottom) just before the start of the range-imaging experiment. These confirm that the core of the jet stream was located over the MU radar site. A vertical shear of horizontal wind can be noticed in the upper part of the jet stream at the altitude of the KH billows. The maximum shear S of 30 m s^{-1} km^{-1} is mainly due to a decrease of the zonal wind component at this altitude. For typical values of N^2 ranging from 10^{-4} rad^2 s^{-2} (in the troposphere) to 4×10^{-4} rad^2 s^{-2} (in the lower stratosphere; e.g., Dalaudier et al. 1994), we find a Richardson number Ri $= N^2/S^2$ between 0.11 and 0.44. Considering that the event occurred in a transition region from the troposphere to the stratosphere, where N^2 can be significantly smaller than 4×10^{-4} rad^2 s^{-2}, the Richardson number may be smaller than 0.25, a condition for triggering the instability. The shear

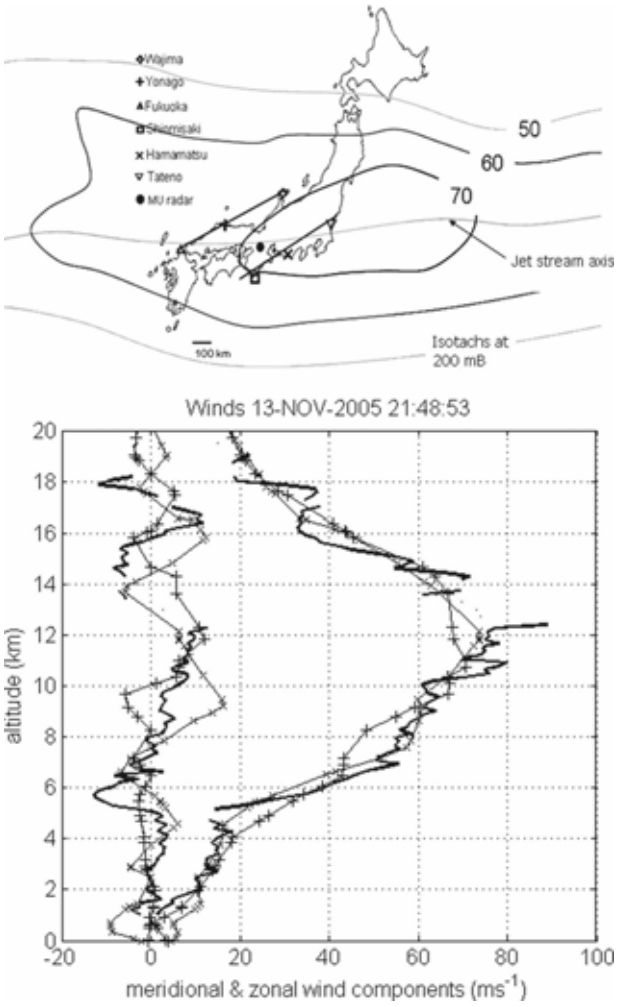

FIG. 3. (top) Positions of the six meteorological stations and MU radar in Japan; Wajima, Yonago, and Fukuoka are roughly aligned, as are Shiomisaki, Hamamatsu, and Tateno. The two short tilted lines indicate the wave front of the IGW observed above the jet stream. Isotachs (m s^{-1}) at 200 hPa at 2100 LT 13 Nov 2005 and the jet axis (light gray line at the center) are also shown. (bottom) Wind component profiles measured by MU radar (solid thick lines) at 2148 LT and by radiosondes launched at Hamamatsu and Yonago. The meridional component is on the lhs and the zonal component on the rhs.

vector is opposite to the wind direction (since wind speed decreased with altitude), compatible with the orientation of the slope of the striations (see Fig. 1; the time axis should be reversed for a spatial representation of the billows, assuming frozen advection).

A more careful inspection of the wind profiles indicates that the zonal and meridional wind profiles inferred by the MU radar reveal wavelike disturbances above 14 km. For an altitude range between 14.18 and 17.87 km, a hodograph analysis (not shown) confirmed the presence of a nearly monochromatic inertia–gravity wave with a vertical wavelength of about 3.5 km. They are commonly found above jet streams, especially in the winter (e.g., Hirota and Niki 1986; Fritts et al. 1988; Sato 1994). The orientation of the major axis was southeast. The ratio R of minor to major axis of the hodograph is estimated between 0.5 and 0.7. The IGW disturbances superimposed on the background field may locally reinforce the horizontal wind shear conducive to the generation of KH instability.

The analysis of data collected from radiosondes released at 2100 LT from the six closest meteorological stations [Wajima at 37.4°N, 136.9°E, hereafter WA; Fukuoka at 33.6°N, 130.4°E, hereafter FU; Shiomisaki at 33.5°N, 135.8°E, hereafter SH; Hamamatsu at 34.8°N, 137.7°E, hereafter HA; Yonago at 35.4°N, 133.3°E, hereafter YO; and Tateno at 36.0°N, 140.1°E, hereafter TA; see also Fig. 3 (top) for their positions] also confirmed the presence of the IGW. Figure 3 shows that the vertical profiles of meridional wind components measured by the radiosondes at HA and YO show similar gross features to those inferred by the MU radar above 14 km with a phase offset compatible with a small inclination (estimated later) of the IGW wave front. The corresponding radiosonde profiles of zonal wind components do not present, however, a clear signature of modulation by an IGW, contrary to the profile provided by the MU radar. We believe that the absence of zonal wind disturbances in the radiosonde data compatible with IGW activity is rather the result of contamination by the strong vertical shear of the westerly jet and an insufficient vertical resolution of the profile than an actual feature of the wind field. The difficulty of retrieving disturbances from a strongly sheared profile has already been emphasized by Sato and Dunkerton (2002), for example.

The observed IGW could be the result of direct radiation from the jet stream, as suggested by Fritts and Luo's (1992) simulations and, in particular, in the cyclonic side of the jet stream in the vicinity of tropopause folds, where the vertical and horizontal shears of horizontal winds are the strongest (Lane et al. 2004; Koch et al. 2005). The aforementioned papers showed that the wave front of the IGW is approximately parallel to the direction of the jet stream. It was possible to check this hypothesis with the present data by analyzing the wind and temperature profiles from the nearby radiosondes in more detail (Fig. 4).

We first tried to separate the background wind and temperature fields from the disturbances produced by the IGW but we did not consider the zonal wind component. For this purpose, the original temperature and meridional wind component profiles were fitted with a low-order polynomial. Figure 4 shows that the tempera-

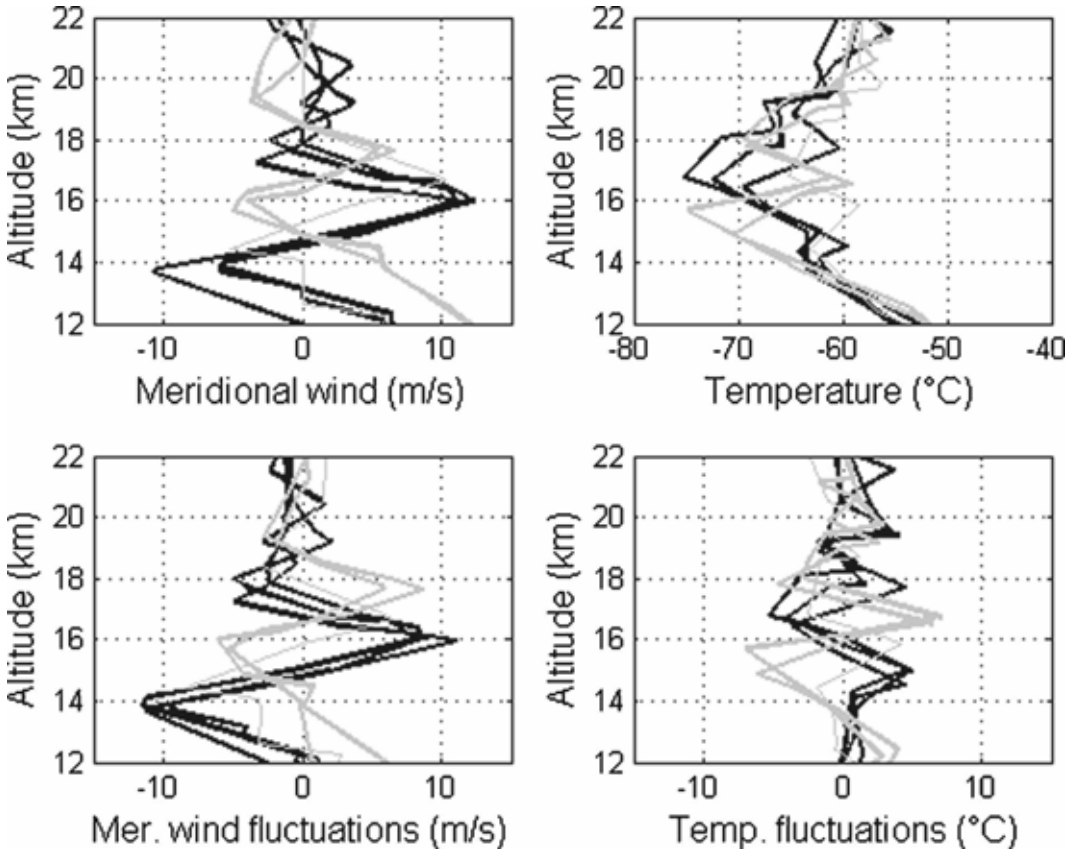

FIG. 4. (top), (left) Meridional wind component and (right) temperature profiles measured from meteorological stations at Shiomisaki, Hamamatsu, and Tateno (black lines) and Fukuoka, Yonago (thick gray lines), and Wajima (thin gray line). The dashed curves represent the background profiles obtained after interpolating the observed profiles with an 8th-order polynomial. (bottom) Same as (top) but only the wind disturbances are represented.

ture fluctuation profiles are in phase at SH, HA, and TA. The same property is observed at FU and YO but not at WA, which is the northernmost station. Also, the temperature fluctuations at SH, HA, TA and at FU and YO are out of phase. These characteristics are compatible with a modulation of the temperature field by an IGW with horizontal wave front roughly oriented along the aligned meteorological stations. This result is in close agreement with the southeast orientation of the major axis of the wind hodograph. It is also noted that similar characteristics are found in the meridional wind fluctuation profiles (Fig. 4), in agreement with the IGW hypothesis. Moreover, it is observed that the temperature fluctuation profiles are not in phase with the wind fluctuation profiles at SH, HA, TA, FU, and YO, as expected from the IGW theory (e.g., Gossard and Hooke 1975).

The minimal distance between the axes formed by SH, HA, TA and FU and YO corresponds to $(2n + 1)/2$ horizontal wavelength (i.e., approximately 300 km for $n = 0$). Thus, a horizontal wavelength of 600 km is consistent with $n = 0$. This value is larger than the estimates proposed by Lane et al. (2004) and Koch et al. (2005) (about 120–250 km) or by Sato (1994) above the MU radar (typically about 200–500 km). However, the latter author also reported values larger than 1000 km. The analysis we now present seems to confirm that a horizontal wavelength of 600 km is the most probable value in the present case.

According to the inertia–gravity wave theory, the ratio R of the minor to major axis of the ellipse, which was estimated at about 0.5–0.7 from the MU radar observation, equals f/ω, where f is the Coriolis parameter ($f = 8.34 \times 10^{-5}$ rad^{-1} at latitude 35°N) and ω is the intrinsic frequency (e.g., Sato 1994). The dispersion equation for nonhydrostatic internal inertia–gravity waves is given by

$$\omega^2 = \frac{N^2k^2 + f^2m^2}{k^2 + m^2},$$

where $m = 2\pi/\lambda_z$is the vertical wavenumber, $k = 2\pi/\lambda_x$ is the horizontal wavenumber, and N is the Brunt–Väisälä frequency. For a typical value of $N^2 = 4 \times 10^{-4}$ rad^2 s^{-2} in the lower stratosphere (e.g., Dalaudier et al. 1994), $\lambda_z = 3.5$ km, and if we select $\lambda_x = 600$ km, we find $\omega = 1.43 \times 10^{-4}$ rad s^{-1}, that is, a period $T = 2\pi/\omega$ of about 12.16 h, typical of inertia–gravity waves at the MU radar latitude (e.g., Sato 1994). Thus, the ratio f/ω is equal to 0.6, fully compatible with the value of R deduced from the hodograph analysis. If we select $\lambda_x =$ 200 km (i.e., $n = 1$), a ratio f/ω of 0.23 is found (i.e., significantly different from R). Using $\lambda_x = 600$ km and $\lambda_z = 3.5$ km, a tilt of the wave front of 0.33° with respect to the horizontal is estimated.

Figure 3 shows the orientation of the wave front as well as isotachs at 200 mb (i.e., approximately at 12 km near the maximum of the jet stream). The wave front and the direction of the mean flow are not aligned, but considering the probable low accuracy of our estimates, this is in quite good agreement with the observations and simulations made by Lane et al. (2004) and Koch et al. (2005) under similar conditions.

4. Conclusions

In the current work, we described coherent turbulent structures with tilted S-like forms resulting from KH instability in the upper part of a jet stream (around 15–16 km). These could be studied using high-resolution reflectivity images obtained with the VHF MU radar (34.85°N, 136.10°E; Japan). The structure's vertical and horizontal extents were estimated to be 0.5–1.0 and 5.3 km, respectively, their ratio being in close agreement with the expected value from the theory of the most unstable wave. The main episode described in detail in the present paper lasted for at least 2 h. The analysis of the vertical velocity fluctuations clearly revealed the presence of a critical level around 15.5 km, confirming the hypothesis of a KH instability. The isotropy of the radar echoes associated with the S-shaped structures suggests that these structures are the signature of coherent billows in a layer of turbulent mixing rather than distorted stable layers such as those observed around 14–15 km, below the KH billows.

From analysis of the horizontal wind and its vertical shear, the KH instability was possibly triggered by an inertia–gravity wave with a period of 12.16 h, and with horizontal and vertical wavelengths of 600 and 3.5 km, respectively. The wave phase lines were found to be roughly parallel to the jet, indicating that the inertia–gravity wave was likely generated by the jet stream and was propagating toward the anticyclonic side of the jet. As such a mechanism can promote the development of bands of turbulent layers in the horizontal plane (Koch et al. 2005), the structures seen by the radar can appear more or less sporadically, depending on the displacement of the mean flow and the direction of propagation of the inertia–gravity wave.

Acknowledgments. The authors thank Dr. François Bertin, Dr. Francis Dalaudier, Prof. M. Yamanaka, and Prof. Michel Crochet for their constructive comments relative to this work. Dr. G. Hassenpflug was supported during this research by a grant from the Japan Society for the Promotion of Science. The MU radar belongs to and is operated by Kyoto University, and is maintained by Mitsubishi Electric Corporation.

REFERENCES

Bertin, F., B. Campistron, J. L. Caccia, and R. Wilson, 2001: Mixing processes in a tropopause folding observed by a network ST radar and lidar. *Ann. Geophys.,* **19,** 953–963.

Browning, K. A., and C. D. Watkins, 1970: Observations of clear air turbulence by high power radar. *Nature,* **227,** 260–263.

Capon, J., 1969: High resolution frequency-wavenumber spectrum analysis. *Proc. IEEE,* **57,** 1408–1418.

Chilson, P. B., A. Muschinski, and G. Schmidt, 1997: First observations of Kelvin-Helmholtz billows in an upper level jet-stream using VHF frequency domain interferometry. *Radio Sci.,* **32,** 1149–1160.

Clark, T. L., W. D. Hall, R. M. Kerr, D. Middleton, L. Radke, F. M. Ralph, P. J. Neiman, and D. Levinson, 2000: Origins of aircraft-damaging clear-air turbulence during the 9 December 1992 Colorado downslope windstorm: Numerical simulations and comparison with observations. *J. Atmos. Sci.,* **57,** 1105–1131.

Dalaudier, F., C. Sidi, M. Crochet, and J. Vernin, 1994: Direct evidence of sheets in the atmospheric temperature field. *J. Atmos. Sci.,* **51,** 237–248.

Fritts, D. C., and Z. Luo, 1992: Gravity wave excitation by geostrophic adjustment of the jet stream. Part I: Two-dimensional forcing. *J. Atmos. Sci.,* **49,** 681–697.

——, T. Tsuda, T. Sato, S. Fukao, and S. Kato, 1988: Observational evidence of a saturated gravity wave spectrum in the troposphere and lower stratosphere. *J. Atmos. Sci.,* **45,** 1741–1759.

Gavrilov, N. M., S. Fukao, H. Hashiguchi, K. Kita, K. Sato, Y. Tomikawa, and M. Fujiwara, 2006: Combined MU radar and ozonesonde measurements of turbulence and ozone fluxes in the tropostratosphere over Shigaraki, Japan. *Geophys. Res. Lett.,* **33,** L09803, doi:10.1029/2005GL024002.

Gossard, E. E., 1990: Radar research on the atmospheric boundary layer. *Radar in Meteorology,* D. Atlas, Ed., Amer. Meteor. Soc., 477–527.

——, and W. H. Hooke, 1975: *Waves in the Atmosphere: Atmospheric Infrasound and Gravity Waves: Their Generation and Propagation*. Elsevier, 456 pp.

Hines, C. O., 1972: Gravity waves in the atmosphere. *Nature,* **239,** 73–78.

Hirota, I., and T. Niki, 1986: Inertia-gravity waves in the stratosphere. *J. Meteor. Soc. Japan,* **64,** 995–999.

Klostermeyer, J., and R. Rüster, 1980: Radar observations and model computation of a jet stream-generated Kelvin-Helmholtz instability. *J. Geophys. Res.,* **85,** 2841–2846.

Koch, S. E., and Coauthors, 2005: Turbulence and gravity waves within an upper-level front. *J. Atmos. Sci.,* **62,** 3885–3908.

Lane, T. P., J. D. Doyle, R. Plougonven, M. A. Shapiro, and R. D. Sharman, 2004: Observations and numerical simulations of inertia-gravity waves and shearing instabilities in the vicinity of a jet stream. *J. Atmos. Sci.,* **61,** 2692–2706.

Luce, H., M. Yamamoto, S. Fukao, D. Hélal, and M. Crochet, 2001: A frequency radar interferometric imaging applied with high resolution methods. *J. Atmos. Sol. Terr. Phys.,* **63,** 221–234.

——, G. Hassenpflug, M. Yamamoto, and S. Fukao, 2006: High-resolution vertical imaging of the troposphere and lower stratosphere using the new MU radar system. *Ann. Geophys.,* **24,** 791–804.

Palmer, R. D., T.-Y. Yu, and P. B. Chilson, 1999: Range imaging using frequency diversity. *Radio Sci.,* **34,** 1485–1496.

Ralph, F. M., P. J. Neimann, and D. Levinson, 1997: Lidar observations of a breaking mountain wave associated with extreme turbulence. *Geophys. Res. Lett.,* **24,** 663–666.

Sato, K., 1994: A statistical study of the structure, saturation, and sources of inertio-gravity waves in the lower stratosphere observed with the MU radar. *J. Atmos. Terr. Phys.,* **56,** 755–774.

——, and T. J. Dunkerton, 2002: Layered structure associated with low potential vorticity near the tropopause seen in high-resolution radiosondes over Japan. *J. Atmos. Sci.,* **59,** 2782–2800.

Shapiro, M. A., 1980: Turbulent mixing within tropopause folds as a mechanism for the exchange of chemical constituents between the stratosphere and troposphere. *J. Atmos. Sci.,* **37,** 994–1004.

Turner, J. S., 1973: *Buoyancy Effects in Fluids*. Cambridge University Press, 367 pp.